Ionics (2021) 27:181–190
https://doi.org/10.1007/s11581-020-03791-3

ORIGINAL PAPER

Effect of K/Zr co-doping on the elevated electrochemical performance of $Na_3V_2(PO_4)_3$/C cathode material for sodium ion batteries

Jiahao Li[1] · Jun Cheng[2,3] · Yanjun Chen[1,2] · Chao Wang[1,2] · Li Guo[2]

Received: 1 April 2020 / Revised: 27 August 2020 / Accepted: 21 September 2020 / Published online: 26 September 2020

Abstract

The $Na_3V_2(PO_4)_3$ (NVP) and its binary-doped $Na_{2.96}K_{0.04}V_{2-x}Zr_{(3/4)x}(PO_4)_3$/C are prepared by a facile solid-phase method. The crystal structure, morphological characteristics, and electrochemical properties are analyzed by XRD, XPS, SEM, and electrochemical tests. The results reveal that K^+ and Zr^{4+} have been successfully doped into NVP system without damaging the original structure. The co-doping strategy can broaden the channels of Na^+ migration to facilitate the ionic conductivities. Meanwhile, it is beneficial to stabilizing the crystal structure effectively by introducing the K^+ and Zr^{4+} with larger ionic radius. All the electrochemical properties of co-doped system are better than that of NVP, resulting from the lager channel for Na^+ diffusion and enhanced intrinsic electrical conductivities by co-doping. Notably, $Na_{2.96}K_{0.04}V_{1.93}Zr_{0.0525}(PO_4)_3$/C exhibits the best electrochemical performance. It delivers a high discharge capacity of 107.3 mAh g^{-1} at 0.1 C; it remains 92.3 mAh g^{-1} after 400 cycles at 2 C, corresponding to the capacity retention of 92.02%; it still maintains 100.0 mAh g^{-1} even at 10 C rate.

Keywords Sodium ion battery · Cathode material · Sodium vanadium phosphate · Co-doping

Introduction

Lithium-ion batteries (LIBs) have attracted significant interest as the power sources of numerous portable consumer electronics due to their high safety, high energy density (both volumetric and gravimetric), long lifetime, wide operating temperature range, and environmental friendliness [1, 2]. However, LIBs cannot meet the ever-increasing marketable demands due to the booming cost and limited availability of lithium reserves [3–6]. It is necessary and significant to develop alternative with high-performance to replace the LIBs. Recently, sodium-ion batteries (SIBs) has been a research hotspot in the fields of energy storage and conversion. Sodium has similar physical and chemical properties with lithium [7, 8], and the abundance is 430 times of lithium resources. Nevertheless, the larger radius of Na^+ is considered to be a restriction because it makes the de-intercalation of Na^+ more difficult and affects the structural stability of host materials. Therefore, the crucial issue in the research of SIBs is to develop the adaptive cathode materials facilitating the migration of Na^+. For the past few years, various cathode materials have been developed and modified, such as $NaVO_3$ [9], $NaFePO_4$ [10–12], $NaVPO_4F$ [13], MnO [14], and $Na_3V_2(PO_4)_3$ [15, 16]. Among the abovementioned electrodes, $Na_3V_2(PO_4)_3$ has generated considerable research interests due to its highly open three-dimensional NASICON structure and the advantages of large capacity and easy preparation [17–19].

$Na_3V_2(PO_4)_3$, with high thermal stability, NASICON structure, and high-power density, is deemed to be one of the most prospective candidates for SIBs. It was firstly proposed by Delmas in 1978. The triclinic $Na_3V_2(PO_4)_3$ is

Jiahao Li and Jun Cheng contributed equally to this work.

Electronic supplementary material The online version of this article (https://doi.org/10.1007/s11581-020-03791-3) contains supplementary material, which is available to authorized users.

✉ Yanjun Chen
yjchen@nuc.edu.cn

✉ Chao Wang
wangchao_nuc@126.com

[1] School of Materials Science and Engineering, North University of China, Taiyuan, China

[2] Advanced Energy Materials and Systems Institute, North University of China, Taiyuan, China

[3] School of Chemical Engineering and Technology, North University of China, Taiyuan, China

constructed by PO_4 tetrahedron and VO_6 octahedron, which has a highly open three-dimensional NASICON structure [20]. The unique crystal structure can be beneficial to the transition of Na^+. However, it suffers from the low intrinsic electronic and ion conductivity [21–23]. Generally, carbon coating is one of the most effective methods to improve the surface electrical conductivity of $Na_3V_2(PO_4)_3$. But it has little effects on the mobility of Na^+ [24, 25]. So, it is significant to search for a solution to realize the rapid and repeated transport of Na^+, improving the electrochemical kinetics and cyclability of SIBs [26]. Cation doping is a successful approach to enhance the bulk phase characteristics. A slight amount of cation ions partially substituting of V in $Na_3V_2(PO_4)_3$, such as Mg [24], Al [25], Ti [26], and Mn [27], have been widely used as alternatively effective methods. In addition, doping K^+ to partially substituting of Na can enhance the stability of the structure and channel [28]. Our previous investigation indicates that the optimum content of the doped K^+ in $Na_{3-x}K_xV_2(PO_4)_3$ is 0.04 (Fig.S1). Therefore, carbon coating combining with cation co-doping may be an effective way to improve electrochemical performance of $Na_3V_2(PO_4)_3$.

In this work, $Na_{2.96}K_{0.04}V_{2-x}Zr_{(3/4)x}(PO_4)_3/C$($x$ = 0.01, 0.04, 0.07, 1) were synthesized by a solid-phase method to enhance the bulk electronic conductivity and ion conductivity. The electrochemical properties of $Na_3V_2(PO_4)_3$ were remarkably improved by the design of carbon coating and K^+/Zr^{4+} co-doping. Conducting carbon coating constructs a conductive network to increase the surface electronic conductivity of particles. Replacing sodium site with potassium can improve the structural stability. In addition, the Zr^{4+} substitution can facilitate the migration of Na^+ by broadening the diffusion pathway of Na^+. Compared with the undoped composite, the co-doped samples exhibit superior cyclic and rate performance owing to the enhanced electrical and ionic conductivity. Notably, $Na_{2.96}K_{0.04}V_{1.93}Zr_{0.0525}(PO_4)_3/C$ composite exhibits the best electrochemical performance: it delivers a high discharge capacity of 107.3 mAh g^{-1} at 0.1 C; it remains 92.3 mAh g^{-1} after 400 cycles at 2 C, corresponding to the capacity retention of 92.02%; it can deliver a high discharge capacity of 100.0 mAh g^{-1} even at 10 C rate.

Experiment

Materials preparation

$Na_{2.96}K_{0.04}V_{2-x}Zr_{(3/4)x}(PO_4)_3/C$($x$ = 0.01, 0.04, 0.07, 0.1) were synthesized by a solid-phase method. ZrO_2, K_2CO_3, Na_2CO_3, $NH_4H_2PO_4$, V_2O_5, and $C_6H_{12}O_6 \cdot H_2O$ were used as raw materials. Carbon-coated design was prepared with $C_6H_{12}O_6 \cdot H_2O$ as carbon source. The raw materials were mixed uniformly with stoichiometric ratio of 9x:0.24:17.76:36:(12-6x):(4-2x). Then, it was ball-milled for 8 h in a high energy ball-milling machine. Afterwards, the yellow fluid was put in the drying box and dried at 80 °C for 12 h. It was ground for 40 min and then calcined at 450 °C for 4 h under argon gas. The active composites, $Na_{2.96}K_{0.04}V_{2-x}Zr_{(3/4)x}(PO_4)_3/C$, were obtained after final heated at 700 °C for 6 h under argon gas. The synthesized samples $Na_{2.96}K_{0.04}V_{2-x}Zr_{(3/4)x}(PO_4)_3/C$ (x = 0, 0.01, 0.04, 0.07, 0.1) were abbreviated as NVP/C, KZ0.01, KZ0.04, KZ0.07, and KZ0.1, respectively.

Characterization

The crystal structure of the materials were determined by X-ray diffraction (XRD, Bruker D8 Advance) with radiation between 10°–80° and a scanning speed of 2° min^{-1}. Scanning electron microscopy (SEM, HITACHI SU8010) and transmission electron microscopy (TEM, JEM-2100F) were used to observe the particle size and morphology. X-ray photoelectron spectroscopy (XPS, ESCALAB 250X) was performed to analyze the binding energies of vanadium, potassium, and zirconium elements. Thermogravimetric analysis (TGA, Mettler-Toledo) was employed to analyze the weight percentages of carbon. The small variation of each doping concentration is determined by inductively coupled plasma-mass spectrometer (ICP-MS) using NexION™ 350D, PerkinElmer (PE), USA.

Electrochemical measurement

The electrochemical properties of the samples were tested on LAND battery test system by button cell (LIR2016). The cathode electrode was prepared by adding 80 wt% active material, 10 wt% acetylene black conductive agent, and 10 wt% polyvinylidene chloride (PVDF) binder to NMP solvent. The mass loading of the active material in each coin cell is about 1.2 mg cm^{-2}. The battery was assembled in a glove box filled with pure argon gas. Both cyclic voltammetry and electrochemical impedance spectroscopy tests were conducted by an electrochemical workstation (AUIVIUM). Cyclic voltammetry was measured at a scan rate of 0.1 m V s^{-1} from 2.4 to 4.1 V. Electrochemical impedance spectroscopy was carried out with an AC amplitude of 10 mV from 0.01 Hz to 100 kHz.

Results and discussion

The XRD patterns of all samples are revealed in Fig. 1a. The vast majority of diffraction peaks can be attributed to the rhombohedral structure with R-3c space group. A few impurity peaks at around 18° are detected, which represent the existence of $NaVP_2O_7$ and $NaVO_2$. These by-products are favorable to improving the conductivity of Na^+ [29, 30]. Moreover, refined results are carried out for all samples to

acquire more accurate information of crystal structure. As shown in Fig. 1b and Fig.S2, the XRD patterns of KZ0.07 sample were clearly assigned to the framework of a rhombohedral NASICON structure with the R3c space group (ICDD#01-078-7289). The Rietveld-refined XRD patterns of KZ0.07 sample are shown in Fig.S3. The refinements are carried out using GSAS program suite, and a space group of R-3c is chosen as the refinement model. The K and Zr elements have substituted at Na1 and V site correspondingly. As can be seen in Table.S1, the occupancy of K and Zr in KZ0.07 sample is 0.0112 and 0.0312, respectively. The sharp peaks with high intensity in Fig. 1b reveal the great crystallinity of KZ0.07 composite. This also demonstrates that co-doping with small amounts of K^+ and Zr^{4+} does not change the crystal structure of $Na_3V_2(PO_4)_3$. Meanwhile, no obvious diffraction peaks of the coated carbon layer are discovered in all samples, which can be attributed to the low content and amorphous state [23]. The refined lattice parameters of KZ0.01, KZ0.04, KZ0.07, KZ0.1, and pure NVP are listed in Table 1 for comparison. The ionic radius of K^+ and Zr^{4+} is apparently larger than those of Na^+ and V^{3+}, suggesting that co-doping can contribute to a bit expanded unit cell volume. The enlarged unit cell volume can broaden the migration pathway of Na^+. Moreover, the ionic radius of Zr^{4+} is very close to V^{3+}, indicating that Zr^{4+} tends to be doped in the V site in NVP. On the other hand, K^+ tends to be doped in the Na site in NVP. Compared with pure NVP, the co-doped composites have larger value of c. Especially, enlarged c parameter by co-doping facilitates the movement of Na^+ during charge and discharge process [24].

To determine the carbon content of NVP/C and KZ0.07 samples, the TGA curves are collected and shown in Fig. 2. The carbon contents of NVP/C and KZ0.07 are 3.92 wt% and 3.77 wt%, respectively. The carbon content of these two samples is about 4 wt%, which can be attributed to the excess carbon source, facilitating the electronic conductivity efficiently. Moreover, the small variation of each doping concentration (0.01, 0.04, 0.07, 0.1) is determined by inductively coupled plasma-atomic spectrometer (ICP-AES). The results are listed in Table.S2. The values of ICP measurements are slightly lower than that of theoretical contents.

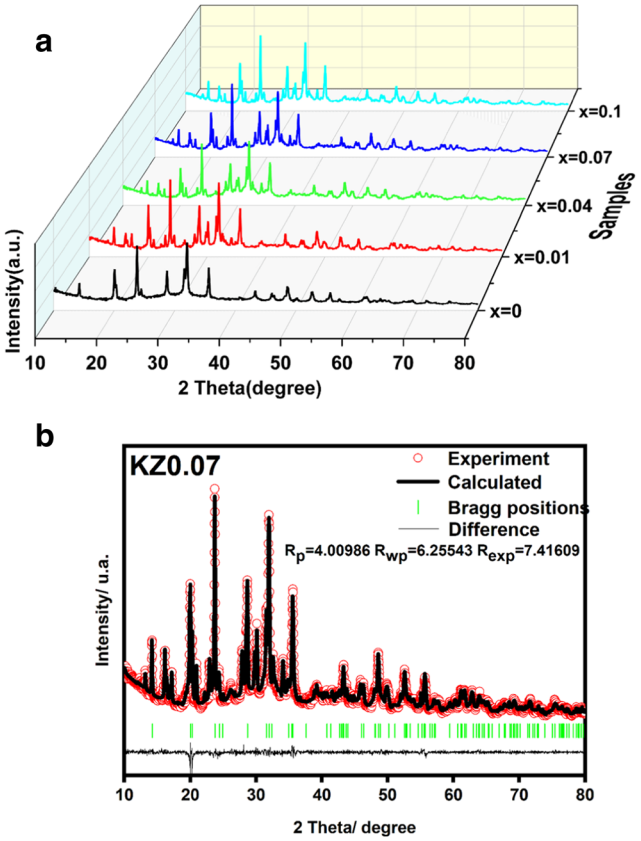

Fig. 1 **a** The XRD patterns of $Na_{2.96}K_{0.04}V_{2-x}Zr_{(3/4)x}(PO_4)_3/C$ (x = 0, 0.01, 0.04, 0.07, 0.1). **b** Rietveld-refined XRD patterns of KZ0.07

The SEM image of pure NVP and co-doped $Na_{2.96}K_{0.04}V_{2-x}Zr_{(3/4)x}(PO_4)_3/C$ (x = 0.01, 0.04, 0.07, 0.1) samples are shown in Fig.S4 and Fig. 3. The different doping amounts of Zr^{4+} result in different morphologies. $Na_{2.96}K_{0.04}V_{2-x}Zr_{(3/4)x}(PO_4)_3/C$ (x = 0.01, 0.04, 0.1) samples display the serious agglomeration with aggregated sizes of up to 9 μm. This phenomenon can be attributed to the high-temperature calcination in the preparation process. Combined with the XRD results (Fig. 1) and refined lattice constants (Table 1), the SEM results indicate that K^+/Zr^{4+} doped into the crystal structure of NVP, which did not destroy the structure stability and had little effects on the particle morphology. In comparison, the particles of KZ0.07 composite are smaller with more

Table 1 The calculated lattice parameters of NVP, KZ0.01, KZ0.04, KZ0.07, and KZ0.1

Sample	a/Å	b/Å	c/Å	V/Å^3	Rexp	Rp	Rwp
NVP	8.7261	8.7261	21.824	1439.18	3.23568	3.09112	3.87253
KZ0.01	8.7266	8.7266	21.903	1440.34	7.48948	4.14126	5.21094
KZ0.04	8.7256	8.7256	21.932	1440.89	7.41609	4.76740	6.25543
KZ0.07	8.7277	87,277	21.942	1441.63	5.33577	4.00986	4.87772
KZ0.1	8.7289	8.7289	21.953	1442.39	7.02946	4.42446	5.55782

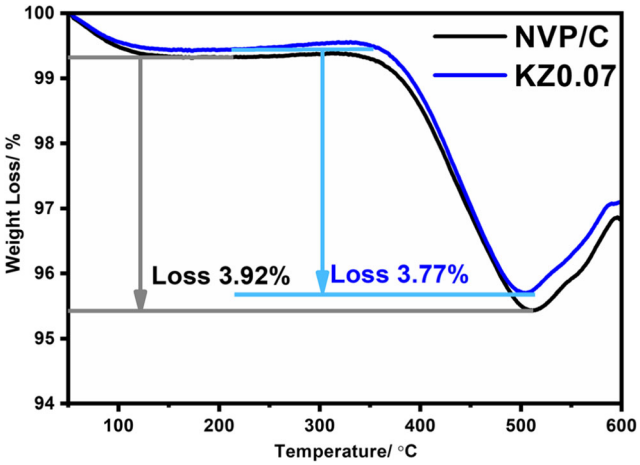

Fig. 2 TGA curves of NVP/C and KZ0.07 samples

even size distribution. The primary size of the KZ0.07 composite is about 2 μm. The reduced particle size can shorten the diffusion path of Na^+ and increase the specific surface area to improve electrochemical performance. The SEM image of KZ0.07 sample at 100 K magnification is shown in Fig. 3e.

HRTEM was used to further elucidate the components in KZ0.07 sample. As displayed in Fig. 4, the surface of particle is covered by a thin carbon layer, which is beneficial to improving the electronic conductivity effectively. This carbonaceous phase is built as a rough layer of 10 nm surrounding the particles. The carbon layer would induce the formation of a mixed conducting network, which is beneficial for both electron and ion transport. In addition, the interplanar spacing of 0.62 nm coincides with the (012) planes in $Na_3V_2(PO_4)_3$ system. The lattice fringes correspond to the well-crystallized structure.

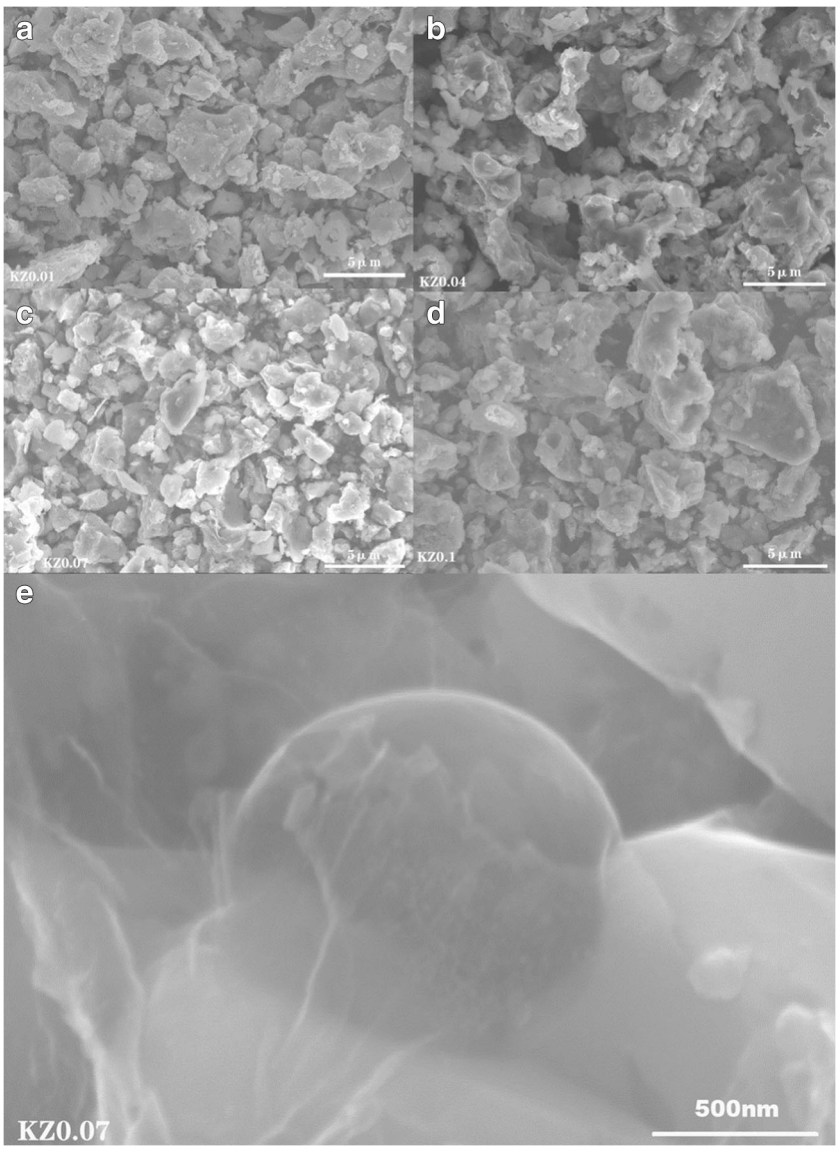

Fig. 3 The SEM images of (**a**) KZ0.01, (**b**) KZ0.04, (**c**) KZ0.07, (**d**) KZ0.1, and (**e**) KZ0.07

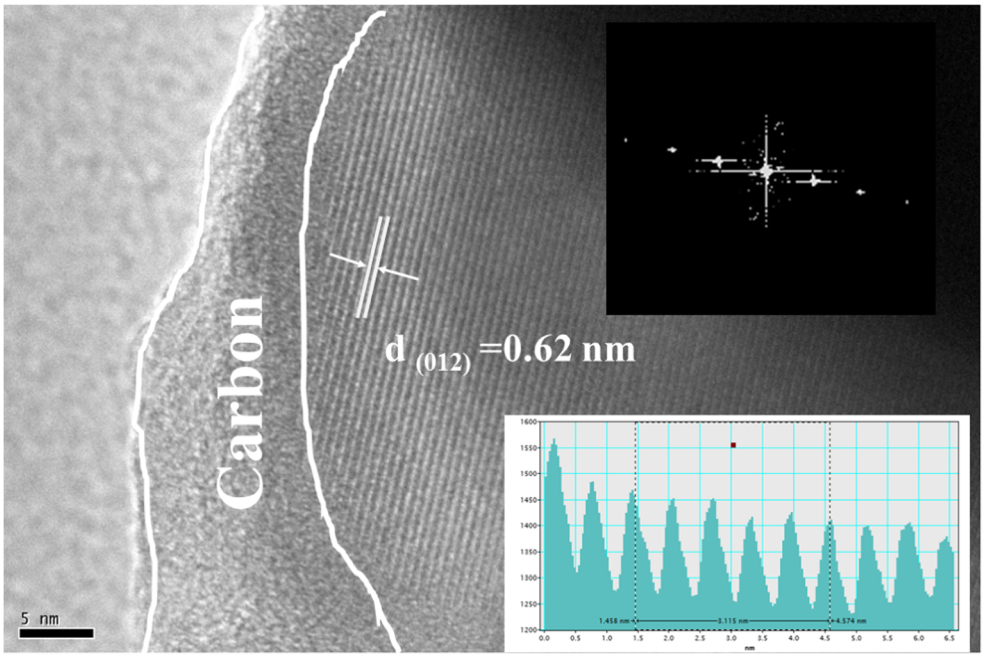

Fig. 4 The HRTEM images of KZ0.07 sample

XPS measurements are conducted to detect elementary binding energy and oxidation state. As shown in Fig. 5a, the C 1s peak is corrected to 284.6 eV for the further study of other elements. The peak at 284.6 eV corresponded to the C 1s can furtherly prove the presence of carbon coating in the sample. The two peaks at 517 eV and 524.15 eV can be attributed to the excitations of V^{3+} $2p_{3/2}$ and V^{3+} $2p_{1/2}$ in KZ0.07 composite, respectively, which are similar to those in reference for the oxidation state of vanadium in NVP without any peak shift [25]. The low-intensity K2p peaks may result from the low doping amount of K^+. As depicted in Fig. 5c, two peaks at binding energy of 295.9 eV and 292.9 eV are corresponding to $K^+2p_{1/2}$ and $K^+2p_{3/2}$. The peaks representing $Zr^{4+}3d_{5/2}$ and $Zr^{4+}3d_{3/2}$ locate at 183.2 eV and 185.65 eV correspondingly. The abovementioned results indicate that both K^+ and Zr^{4+} have successfully doped into Na site and V site in KZ0.07 sample. Co-doping of K^+ and Zr^{4+} in samples and the maintenance of V^{3+} suggest that vacancies can be produced in V site. Appropriate vacancies are in favor of rapid transport for Na^+ in electroactive-doped particles. The specific fitting results are listed in Table 2.

Table 2 The XPS fitting results of the sample

Core line	Peaks	Binding energy (eV)
V2 p	V^{3+} 2p3/2	517.00
	V^{3+} 2p1/2	524.15
K 2 p	K^+ 2p3/2	295.90
	K^+ 2p1/2	292.90
Zr 3 d	Zr^{4+} 3d5/2	185.65
	Zr^{4+} 3d3/2	183.20

The cyclic voltammetry curves of all samples are displayed in Fig. 6. The scanning speed was 0.1 mVs^{-1} and the scan voltage range was 2.3–4.1 V. The CV curves of all samples are composed of one oxidation peak and two reduction peaks, which corresponds to the extraction and insertion of Na^+. The curves reveal similar, indicating that Na^+ and Zr^{4+} co-doping does not change the electrochemical reaction process of NVP. It is also clearly reflected the intercalation and extraction processes of Na^+. For comparison, the co-doped samples have redox peaks with higher intensity and larger areas, suggesting larger electrochemical capacity. Especially, the extra occurrence of a small reversible redox couple at 3.7 V is observed in the co-doped samples, corresponding to the partial redox reaction of V^{4+}/V^{5+}. This consequence is discovered in the related doped NVP composites, such as $Na_3V_{1.98}(PO_4)_3/C$ [29] and $Na_3V_{1.98}(PO_4)_{2.9}F_{0.3}/C$ [30].

Figure 7 a and b show the galvanostatic charge/discharge curves of NVP/C and $Na_{2.96}K_{0.04}V_{2-x}Zr_{(3/4)x}(PO_4)_3/C(x$ = 0.01, 0.04, 0.07, 0.1) in the first cycle at 0.1 C and 2 C, respectively. As shown in Fig. 7a, all the samples exhibit one discharge plateau at 3.4 V, which can be assigned to the intercalation/deintercalation of Na^+ at M2 site. Notably, the K/Zr co-doped samples reveal a new voltage platform at around 3.7 V, corresponding to the V^{4+}/V^{5+} reaction resulting from the reversible extraction of the third Na^+ at M1site [30–33]. The initial discharge capacities at 0.1C rate of NVP/C, KZ0.01, KZ0.04, KZ0.07, and KZ0.1 are 94.5, 91, 100.3, 107.3, and 97.1 mAh g^{-1}, respectively. When it turns to be 2 C rate, the values are 85.6, 91.2, 96, 107.1, and 93.5 mAh g^{-1}. Moreover, the KZ0.07 composite exhibits the exceedingly

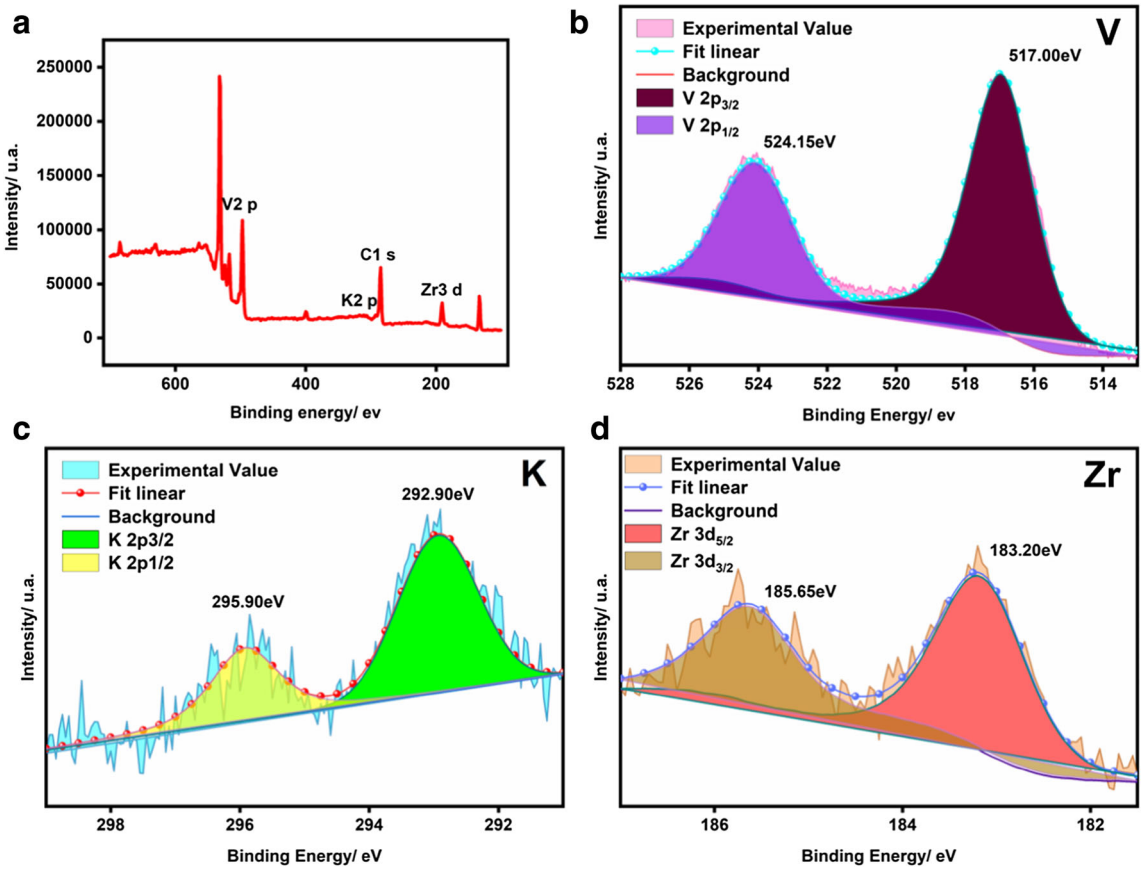

Fig. 5 The XPS spectra of KZ0.07 sample

slight polarization voltage, indicating the favorable reversibility of Na^+ migration. It indicates that the co-doping of K^+ and Zr^{4+} can enhance the charge and discharge characteristics significantly. All the doped samples reveal the typical voltage plateaus of NVP with lower polarization voltage than that of the NVP/C sample, which can be attributed to the enlarged diffusion pathway caused by K^+ and Zr^{4+} co-doping, inducing the fast insertion and extraction of sodium-ion.

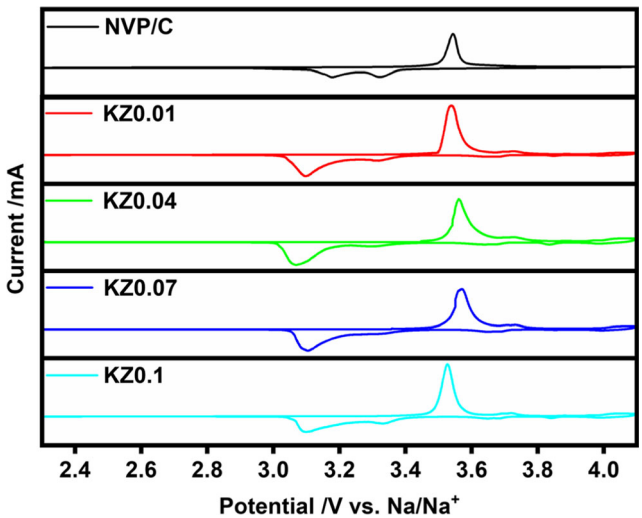

Fig. 6 Cyclic voltammograms of $Na_{2.96}K_{0.04}V_{2-x}Zr_{(3/4)x}(PO_4)_3/C$ (x = 0.01, 0.04, 0.07, 0.1) and pure NVP at 0.1 mV s^{-1}

Figure 7c exhibits the cycling performances of all samples at 2 C in the voltage range of 2.4–4.1 V. KZ0.07 composite possesses the best cyclability among the abovementioned materials. The highest initial discharge capacity is 100.3 mAh g^{-1}, and it remains 92.3 mAh g^{-1} after 400 cycles, corresponding to the capacity retention of 92.02%. By comparison, NVP/C sample only has the 77.5 mAh g^{-1} after a cycle and the capacity retention is about 76.5%. The coulombic efficiency of KZ0.07 maintains in 99.93% during the 400 cycles at 2 C rate, suggesting the good reversibility. Moreover, the 400th charge/discharge curves of all samples are displayed in Fig. 7d. Obviously, the value of polarization voltage for NVP/C has greatly increased, leading to the poor electrochemical property. The tiny plateau at 3.7 V representing the reaction of V^{4+}/V^{5+} has gradually disappeared for KZ0.01, KZ0.04, and KZ0.1. However, it still contributes some capacity for the KZ0.07 composite. The improved cycle performance of KZ0.07 mainly relates with the large and stable channels for the extraction/insertion of Na^+, which can be ascribed to the co-doping of K^+ and Zr^{4+}. This result can correspond to the XRD results. A small amount of cationic co-doping can enlarge the ionic transfer channel of NVP to improve the electrochemical performance. In a certain range, the

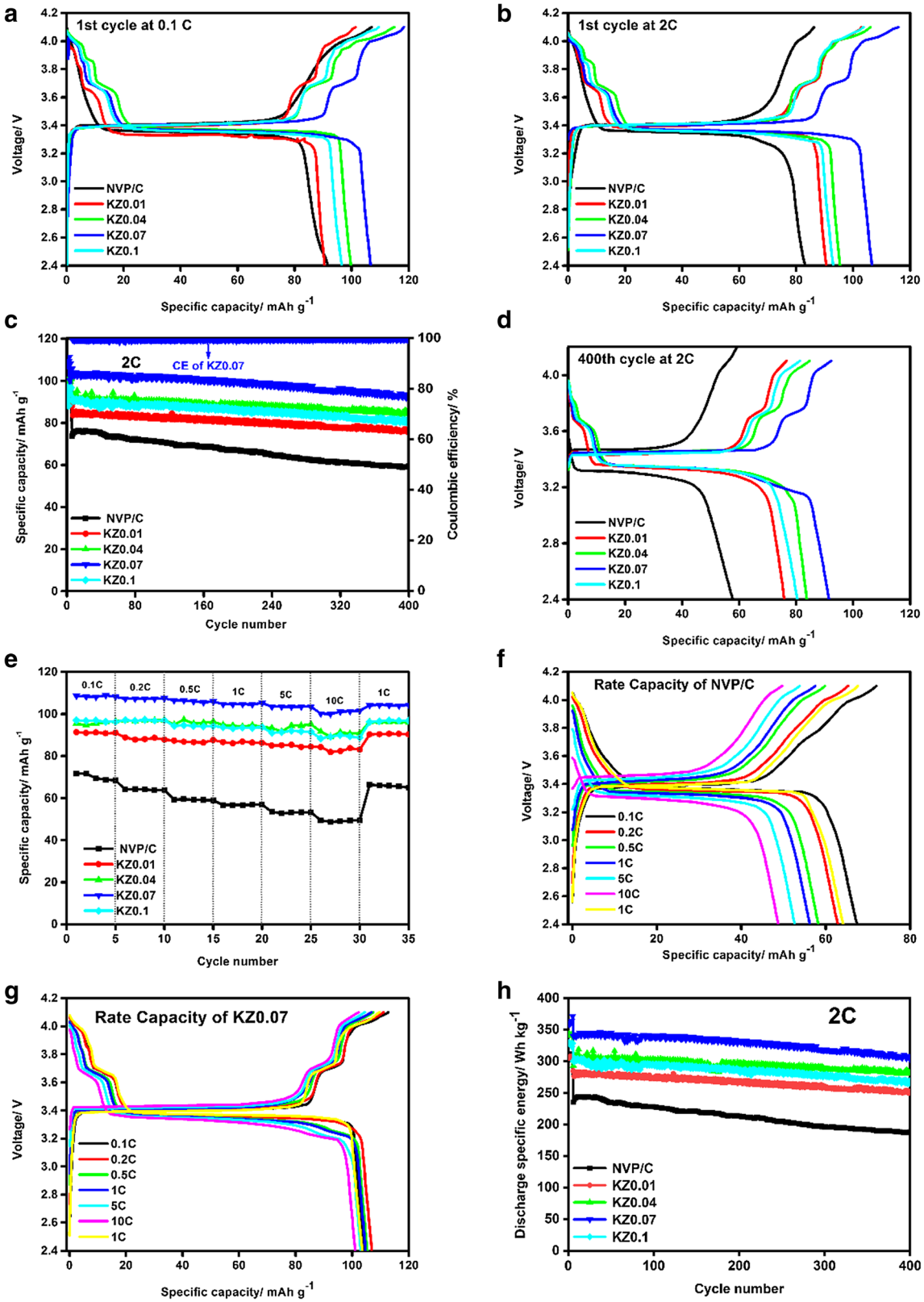

Fig. 7 **a** First cycle of charge/discharge curves of all samples at 0.1 C. **b** First cycle of charge/discharge curves of all samples at 2 C. **c** Long-cycle performance of all samples at 2 C for 400 cycles. **d** 400th cycle charge/discharge curves of all samples at 2 C. **e** Rate performance of all samples. Charge/discharge curves at different densities for NVP/C (**f**) and KZ0.07-NVP/C (**g**) samples. **h** Discharge specific energy curves for all samples at 2C

Table 3 The calculated sodium diffusion coefficients of all composites

Samples	R_{ct} (ohm)	D_{Na^+} ($cm^2 \cdot s^{-1}$)
NVP	1246.68	1.59×10^{-15}
KZ0.01	584.70	8.54×10^{-15}
KZ0.04	650.90	8.83×10^{-15}
KZ0.07	386.79	1.15×10^{-14}
KZ0.1	444.52	1.03×10^{-14}

electrochemical performance of NVP can be improved with the increase of doping amount because of the larger channel and more suitable amounts of vacancies. However, when the excess cations take up the position of the sites, the cell shrinkage occurs and the transport channel compresses, which impedes the rapid diffusion of Na^+ in the bulk of electroactive material and is unfavorable for the enhancement of structural stability.

In order to investigate the influence of K^+ and Zr^{4+} co-doping on the rate capability, NVP/C and $Na_{2.96}K_{0.04}V_{2-x}Zr_{(3/4)x}(PO_4)_3/C$ ($x = 0.01, 0.04, 0.07, 0.1$) samples were charged and discharged at diverse density from 0.1 to 10 C then back to 1 C. Figure 7e shows that discharge capacities of undoped NVP/C electrode are much lower than that of KZ0.07 at the same measured rates. When NVP/C discharges at 0.1, 0.2, 0.5, 1, 5, 10, and 1 C, its discharge capacities are 69.5, 64.1, 59.3, 56.8, 53.1, 49.0, and 65.5 mAh g^{-1}. Its reversible capacity drops rapidly with the increase of current rates. The capacity retention ratio at 10 C is 70.50%. While KZ0.07 composite presents a significantly enhanced rate capability and exhibits discharge capacities as high as 108.2, 107.2, 106.0, 104.6, 103.4, 100.0, and 104.2 mAh g^{-1} at 0.1, 0.2, 0.5, 1, 5, 10, and 1 C, respectively. The capacity retention ratio at 10 C corresponds to 92.42% of that at 0.1 C. The outstanding electrochemical performance of KZ0.07 at different current rates was attributed to the introduction of K^+ and Zr^{4+} which is beneficial to the fast Na^+ diffusion, especially at high current rates. For further investigation of the rate capability, the charge/discharge curves at different current densities for NVP/C and KZ0.07 are revealed in Fig. 7f and g. The high overlap ratio of curves in Fig. 7g for KZ0.07 demonstrates the excellent reversible capability even at high current densities. By contrast, the front opening of curve in Fig. 7f for NVP/C gets larger with the increase of current density, which suggests the poorer electrochemical property. Due to the appearance of higher platform at 3.7 V for the co-doped samples, the specific energy must be improved accordingly. As shown in Fig. 7h, the discharge specific energy of NVP/C is 241.3 Wh kg^{-1}, much lower than that of the co-doped composites. KZ0.07 exhibits the highest value of 349.5 Wh kg^{-1} at 2 C rate. The elevated energy density is ascribed to the enhanced capacity and potential.

To further understand the effects of co-doping of K^+ and Zr^{4+} on the electrochemical behaviors, electrochemical impedance spectroscopy (EIS) tests were performed on $Na_{2.96}K_{0.04}V_{2-x}Zr_{(3/4)x}(PO_4)_3/C$ ($x = 0.01, 0.04, 0.07, 0.1$) composites and pure NVP/C. Figure 8 shows that all composites possess typical Nyquist characteristics. The linear relationship of Z_{re} and $\omega^{-1/2}$ based on the low frequency region is shown in Fig. 8b. The Na^+ diffusion coefficients (D_{Na+}) are calculated according to the equation:

$$Z_{re} = R_s + R_{ct} + \sigma\omega^{-0.5} \quad (1)$$

$$D = R^2T^2/2A^2n^4F^4C_{Na}{}^2\sigma^2 \quad (2)$$

where σ is the Warburg factor, which is associated with Z_{re} in Eq. (1). Additionally, ω, R, T, A, n, F, and C_{Na} are frequency, gas constant, absolute temperature, surface area of the cathode, number of electrons per molecule during oxidization, Faraday constant, and the concentration of sodium ions (3.47×10^{-3} mol cm^{-3}), respectively. The relationship of Z_{re} and $\omega^{-1/2}$ can be fitted by a straight line whose slope is σ in Eq. (2). The calculated $D_{Na}{}^+$ is listed in Table 3. The $D_{Na}{}^+$ of KZ0.07 composite is approximately one order of magnitude higher than that of NVP/C. The increased $D_{Na}{}^+$ may be owing to the slightly enlarged unit cell volume, which expands the Na^+ migration pathway and facilitates the insertion/extraction of Na^+. Moreover, the charge transfer resistance of $Na_{2.96}K_{0.04}V_{2-x}Zr_{(3/4)x}(PO_4)_3/C$($x = 0.01, 0.04, 0.07, 0.1$) is significantly lower than that of the pure NVP/C sample. It

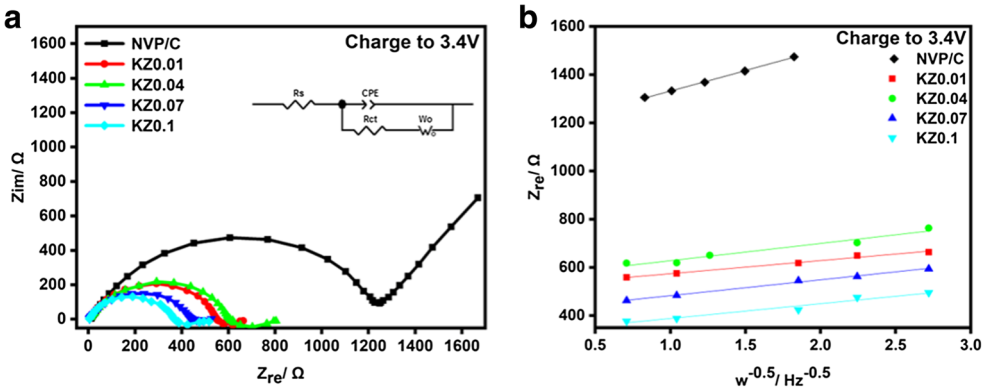

Fig. 8 **a** Nyquist plots and fitting curves of $Na_{2.96}K_{0.04}V_{2-x}Zr_{(3/4)x}(PO_4)_3/C$ ($x = 0.01, 0.04, 0.07, 0.1$) and pure NVP at the initial state. **b** The corresponding profiles of the relationship between Z_{re} and $\omega^{-1/2}$

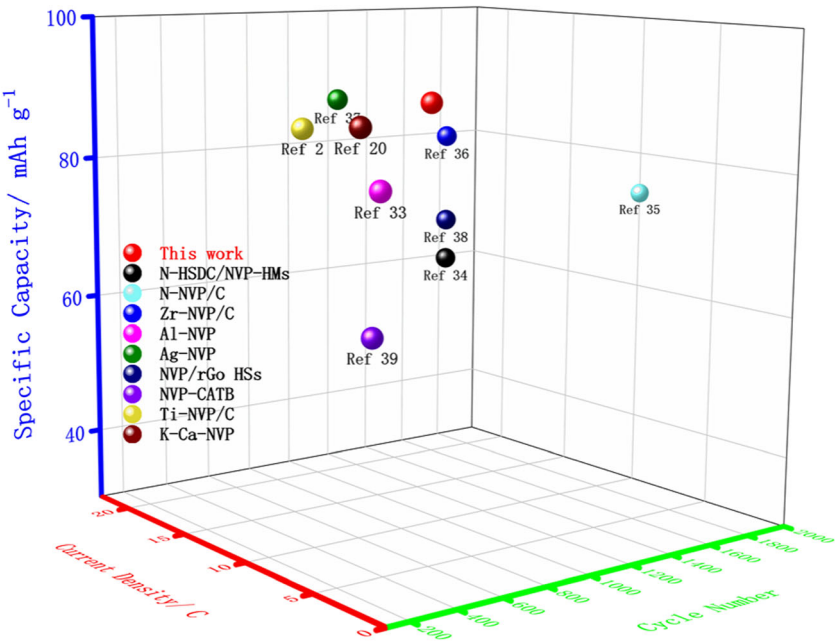

Fig. 9 Comparison of specific capacity of modified samples

means that the doped K^+ and Zr^{4+} can significantly improve the apparent and intrinsic electrical conductivities of NVP. In particular, the lowest Rct value of KZ0.07 suggests that it has the best electrochemical properties among all the samples, which is in accordance with the results in Fig. 7.

In addition, we compared the electrochemical performance of KZ0.07 with modified NVP materials by other teams in recent years [34–39]. As shown in Fig. 9, it is obvious that the KZ0.07 prepared by this work has the highest specific discharge capacity after a long cycle at a high rate, indicating that it has an excellent electrochemical property.

Conclusions

In summary, the modified $Na_{2.96}K_{0.04}V_{2-x}Zr_{(3/4)x}(PO_4)_3/C$($x$ = 0.01, 0.04, 0.07, 0.1) composites have been prepared by a solid-phase method in this study. The investigation of influence resulted from doped K^+ and Zr^{4+} on the $Na_3V_2(PO_4)_3$ is explored in detail. The physicochemical and electrochemical performances for the obtained powders are analyzed by XRD, XPS, SEM, CV, and EIS. The results indicate that the co-doping does not destroy the crystal structure of $Na_3V_2(PO_4)_3$. The co-doped strategy can not only expand and stabilize the migration pathway of Na^+ but also improve the apparent and intrinsic electrical conductivities. Accordingly, the co-doped materials exhibit better electrochemical performance than that of the undoped one. Especially, KZ0.07 composite shows the best performance among all the co-doped systems. Hence, the K^+ and Zr^{4+} co-doping and combining with carbon coating have a practical application prospect to synthesize the high-rate and long-life $Na_3V_2(PO_4)_3$ for SIBs.

Acknowledgments The authors thank Hengcong Qin from Shiyanjia Lab (www.shiyanjia.com) for the XRD and XPS analysis.

Funding The present work is financially supported by Natural Science Foundation of Shanxi Province (No.201901D211217, No.201801D121284), Scientific and Technological Innovation Programs of Higher Education Institutions in Shanxi (STIP), Major Science and Technology Projects of Shanxi Province (No.20181102018), and Program for the Innovative Talents of Higher Education Institutions of Shanxi (PTIT).

References

1. Wang C, Li ZH, Liu HM, Wang YG (2017) Improved electrochemical performance of a $Li_3V_2(PO_4)_3$ cathode in a wide potential window for lithium-ion storage by surface N-doped carbon coating and bulk K-doping. New J Chem 41(17):8772–8780
2. Oh RG, Hong JE, Jung HW, Ryu KS (2015) Electrochemical properties of $Li_{3-x}Na_xV_{2-x}Ti_x(PO_4)_3/C$ cathode materials in lithium ion batteries. J Power Sources 295:1–8
3. Larcher D, Tarascon JM (2015) Towards greener and more sustainable batteries for electrical energy storage. Nat Chem 7(1):19–20
4. Byoungwoo K, Gerbrand C (2009) Battery materials for ultrafast charging and discharging. Nature 458(190-193)
5. Song HK, Lee KT, Kim MG, Nazar LF, Cho J (2010) Recent progress in nanostructured cathode materials for lithium secondary batteries. Adv Funct Mater 20(23):3818–3834
6. Slater MD, Kim D, Lee E, Johnson C (2013) Sodium ion batteries. Adv Funct Mater 23(8):947–958
7. Palomares V, Serras P, Villaluenga I, Hueso KB, Carretero-Gonzalez J, Rojo T (2012) Na-ion batteries, recent advances and present challenges to become low cost energy storage systems. Energy Environ Sci 5(3):5884–5901

8. Raju V, Rains J, Gates C, Luo W, Wang XF, Stickle WF, Stucky GD, Ji XL (2014) Superior cathode of sodium-Ion batteries: orthorhombic V_2O_5 nanoparticles generated in nanoporous carbon by ambient hydrolysis deposition. Nano Lett 14(7):4119–4124
9. Ali G, Islam M, Jung HG, Nam KW, Chung KY (2018) Probing the sodium insertion/extraction mechanism in a layered $NaVO_3$ anode material. ACS Appl Mater Interfaces 10(22):18717–18725
10. Liu YC, Zhang N, Wang FF, Liu XB, Jiao LF, Fan LZ (2018) Approaching the downsizing limit of maricite $NaFePO_4$ toward high-performance cathode for sodium-ion batteries. Adv Funct Mater 28(30):1801917
11. Kim J, Seo DH, Kim H, Park I, Yoo JK, Jung SK, Park YU, Goddard WA, Kang K (2015) Unexpected discovery of low-cost maricite $NaFePO_4$ as a high-performance electrode for Na-ion batteries. Energy Environ Sci 8(2):540–545
12. Oh SM, Myung ST, Hassoun J, Scrosati B, Sun YK (2012) Reversible $NaFePO_4$ electrode for sodium secondary batteries. Electrochem Commun 22:149–152
13. Ling MX, Li F, Yi HM, Li XF, Hou GJ, Zheng Q, Zheng HM (2018) Superior Na-storage performance of molten-state-blending-synthesized monoclinic $NaVPO_4F$ nanoplates for Na-ion batteries. J Mater Chem A 6(47):24201–24209
14. He YZ, Xu P, Zhang B, Du YC, Song B, Han XJ, Peng HS (2017) Ultrasmall MnO nanoparticles supported on nitrogen-doped carbon nanotubes as efficient anode materials for sodium ion batteries. ACS Appl Mater Interfaces 9(44):38401–38404
15. Jian ZL, Zhao L, Pan HL, Hu YS, Li H, Chen W, Chen LQ (2012) Carbon coated $Na_3V_2(PO_4)_3$ as novel electrode material for sodium ion batteries. Electrochem Commun 14(1):86–89
16. Saravanan K, Mason CW, Rudola A, Wong KH, Balaya P (2013) The first report on excellent cycling stability and superior rate capability of $Na_3V_2(PO_4)_3$ for sodium ion batteries. Adv Energy Mater 3(4):444–450
17. Cheng SQ, Wu C, Shen LF, Zhu CB, Huang YY, Maier J, Yu Y (2017) Challenges and perspectives for NASICON-type electrode materials for advanced sodium-ion batteries. Adv Mater 29(48): 1700431
18. Noguchi Y, Kobayashi E, Plashnitsa LS, Okada S, Yamaki J (2013) Fabrication and performances of all solid-state symmetric sodium battery based on NASICON-related compounds. Electrochim Acta 101(SI):59–65
19. Jian ZL, Han WZ, Lu X, Yang HX, Hu YS, Zhou J, Zhou ZB, Li JQ, Chen W, Chen DF, Chen LQ (2013) Superior electrochemical performance and storage mechanism of $Na_3V_2(PO_4)_3$ cathode for room-temperature sodium-ion batteries. Adv Energy Mater 3(2): 156–160
20. Zhu Q, Cheng H, Zhang XM, He LQ, Hu LZ, Yang JW, Chen QQ, Lu ZG (2018) Improvement in electrochemical performance of $Na_3V_2(PO_4)_3$/C cathode material for sodium-ion batteries by K-Ca co-doping. Electrochim Acta 281:208–217
21. Guo J-Z, Wu X-L, Wan F, Wang J, Zhang XH, Wang RS (2015) A superior $Na_3V_2(PO_4)_3$ based nanocomposite enhanced by both N-doped coating carbon and graphene as the cathode for sodium-ion batteries. Chem-Eur J 21(48):17371–17378
22. Li X, Huang YY, Wang JS, Miao L, Li YY, Liu Y, Qin YG, Fang C, Han JT, Huang YH (2018) High valence Mo-doped $Na_3V_2(PO_4)_3$/C as a high rate and stable cycle-life cathode for sodium battery. J Mater Chem A 6(4):1390–1396
23. Wang EH, Xiang W, Rajagopalan R, Wu ZG, Yang JH, Chen MZ, Zhong BH, Dou SX, Chou SL, Guo XD, Kang YM (2017) Construction of 3D pomegranate-like $Na_3V_2(PO_4)_3$/conducting carbon composites for high-power sodium-ion batteries. J Mater Chem A 5(20):9833–9841
24. Li H, Yu XQ, Bai Y, Wu F, Wu C, Liu LY, Yang XQ (2015) Effects of Mg doping on the remarkably enhanced electrochemical performance of $Na_3V_2(PO_4)_3$ cathode materials for sodium ion batteries. J Mater Chem A 3(18):9578–9586
25. Chen YJ, Xu YL, Sun XF, Wang C (2018) Effect of Al substitution on the enhanced electrochemical performance and strong structure stability of $Na_3V_2(PO_4)_3$/C composite cathode for sodium-ion batteries. J Power Sources 375:82–92
26. Zhang B, Zeng T, Liu Y, Zhang JF (2018) Effect of Ti-doping on the electrochemical performance of sodium vanadium(III) phosphate. RSC Adv 8(10):5523–5531
27. Shen W, Li H, Guo ZY, Li ZH, Xu QJ, Liu HM, Wang YG (2016) Improvement on the high-rate performance of Mn-doped $Na_3V_2(PO_4)_3$/C as a cathode material for sodium ion batteries. RSC Adv 6(75):71581–71588
28. Lim SJ, Han DW, Nam DH, Hong KS, Eom JY, Ryu WH, Kwon HS (2014) Structural enhancement of $Na_3V_2(PO_4)_3$/C composite cathode materials by pillar ion doping for high power and long cycle life sodium-ion batteries. J Mater Chem A 2(46):19623–19632
29. Chen YJ, Xu YL, Sun XF, Li L, Li L (2018) Off-stoichiometric $Na_3V_{2-x}(PO_4)_3$/C cathode composites with stable lifetime for sodium ion batteries. Ceram Int 44:13055–13064
30. Chen YJ, Xu YL, Sun XF, Zhang BF, He SN, Wang C (2018) F-doping and V-defect synergetic effects on $Na_3V_2(PO_4)_3$/C composite: a promising cathode with high ionic conductivity for sodium ion batteries. J Power Sources 397:307–317
31. Aragon MJ, Lavela P, Ortiz GF, Tirado JL (2015) Effect of iron substitution in the electrochemical performance of $Na_3V_2(PO_4)_3$ as cathode for Na-ion batteries. J Electrochem Soc 162:3077–3083
32. Aragon MJ, Lavela P, Ortiz GF, Tirado JL (2015) Benefits of chromium substitution in Na3V2(PO4)(3) as a potential candidate for sodium-ion batteries. Chemelectrochem 2(7):995–1002
33. Ana C, Pedro L, Tirado JL, Perez-Vicente C (2020) Increasing energy density with capacity preservation by aluminum substitution in sodium vanadium phosphate. ACS Appl Mater Inters 12(19): 21651–21660
34. Sun K, Hu YB, Zhang XD, Hui KS, Zhang KL, Xu GG, Ma JY, He W (2020) N-doped hard soft double-carbon-coated $Na_3V_2(PO_4)_3$ hybrid-porous microspheres with pseudocapacitive behaviour for ultrahigh power sodium-ion batteries. Electrochim Acta 335: 135680
35. Hu FD, Jiang XL (2020) A stable and superior performance of $Na_3V_2(PO_4)_3$/C nano composites as cathode for sodium-ion batteries. Inorg Chem Commun 115:107860
36. Ma HY, Zhao BC, Bai J, Li KZ, Fang ZT, Wang PY, Li WY, Zhu XB, Sun YP (2020) Improved electrochemical performance of $Na_3V_{2-x}Zr_x(PO_4)_{(3)}$/C through electronic and ionic conductivities regulation. J Electrochem Soc 167(7):070548
37. Hong XD, Huang XB, Ren YR, Wang HY, Ding X, Jin JL (2020) Superior Na-storage performance of $Na_3V_2(PO_4)_{(3)}$/C-Ag composites as cathode material for Na-ion battery. J Alloys Compd 822: 153587
38. Xu JY, Gu EL, Zhang ZZ, Xu ZH, Xu YF, Du YC, Zhu XS, Zhou XS (2020) Fabrication of porous NagV2(P04)3/reduced graphene oxide hollow spheres with enhanced sodium storage performance. J Colloid Interface Sci 567:84–91
39. Salehi AH, Masoudpanah SM, Hasheminiasari M, Yaghtin A, Safanama D, Ong CK, Reddy MV, Adams S (2020) A solution synthesis of $Na_3V_2(PO_4)_3$ cathode for sodium storage by using CTAB additive. Solid State Ionics 347:115269